Experimental identification of fracture toughness of a carbon black-filled styrene butadiene rubber undergoing energy dissipation by Mullins softening

David Roucou, Julie Diani, Mathias Brieu, Davide Colombo

Available online at www.sciencedirect.com
ScienceDirect
Mechanics of Materials 00 (2020) 1–17
MOM

Experimental identification of fracture toughness of a carbon black-filled styrene butadiene rubber undergoing energy dissipation by Mullins softening

David Roucou[a,b], Julie Diani[c,*], Mathias Brieu[b,d], Davide Colombo[a]

[a] *Manufacture Française des Pneumatiques Michelin, CERL, Ladoux, 63040 Clermont-Ferrand, France*
[b] *Univ. Lille, CNRS, Centrale Lille, UMR 9013 - LaMcube - Laboratoire de Mécanique, Multiphysique, Multi-échelle, F-59000 Lille, France*
[c] *Laboratoire de Mécanique des Solides, CNRS UMR 7649, École Polytechnique, Institut Polytechnique de Paris, Route de Saclay, 91128 Palaiseau, France*
[d] *College ECST, California State University-Los Angeles, USA*

Abstract

The impact of the loading history on the resistance to break of a carbon-black filled styrene butadiene rubber is explored experimentally. Carbon-black filled rubberlike materials soften significantly upon the first loading due to the well known Mullins effect. The impact of this effect on the critical energy release rate at break, G_c, of the considered material is quantitatively estimated. For this purpose, the classical notched pure shear geometry is considered and the seminal global analysis from Rivlin and Thomas (1953) is adopted. Moreover, the same analysis is extended to non-elastic materials in order to account for the Mullins softening and define the critical energy release rate, G_c^*, characterizing the creation of new crack surfaces without including the energy dissipated by Mullins softening. Both global quantities, G_c and G_c^*, appear decreasing with the increase of softening already undergone by the material, stressing the difficulty of proposing a predictive criterion for the material resistance to failure. Finally, thanks to the local measures of the strain fields on the free surface of the pure shear specimen just before the crack propagation, it has been possible to evaluate the amount of Mullins dissipation upon the crack propagation and to explore the possible existence of an intrinsic value, G_0, characterizing the crack propagation independently of any other source of dissipation.

Keywords: Fracture, Toughness, Pure shear, Mullins effect, Rubber

1. Introduction

The strength of elastomers can be affected by the presence of cracks initiated during use by fatigue or accidentally by sharp objects. The growth of pre-existing cracks has been studied for several decades, following the seminal work of Rivlin and Thomas (1953). These authors proposed an energy fracture criterion defined as an extension of the linear elastic fracture mechanics Griffith criterion (Griffith, 1921). The latter applies to non-dissipative elastic materials only and was extended to rubbers under the assumption that any source of energy dissipation is confined in the crack tip vicinity, and can therefore be neglected in the global energy balance. This assumption was experimentally verified by Rivlin and Thomas (1953) on non-filled natural rubbers. It allows calculating the energy release rate, commonly noted G, which designates the decrease in total potential energy per increase of crack surface area. In a structure, when G reaches a material critical energy release rate G_c, the crack propagates creating new surfaces. Therefore, when G can be determined, the growth of a crack can be predicted independently of the specimen shape or size.

*Corresponding author. Tel. : + 33 1 69 33 57 93
Email address: julie.diani@polytechnique.edu (Julie Diani)

The energy criterion such as defined by Rivlin and Thomas (1953) has been commonly used for filled rubbers (Glucklich and Landel, 1976; Medalia, 1987; De and Gent, 1996; Hamed and Park, 1999; Gherib et al., 2010 among others), and G_c is often asserted on a pure shear geometry, which provides a simple analysis and reliable values (Roucou et al., 2019). However, carbon-black filled elastomers undergo significant softening when first submitted to a level of strain never applied before, due to the well known Mullins effect (Mullins, 1969; Diani et al., 2009). The phenomenon is rate independent and induces energy dissipation due to the degradation of the bonded layer around the carbon-black particles (Diaz et al., 2014). Therefore, when considering a notched pure shear sample of such a material, submitted to a monotonic loading, the energy dissipation cannot be considered localized to the vicinity of the crack tip only. Recently, Qi et al. (2018) have proposed a theoretical framework to account for bulk energy dissipation for mode-I plane stress cracks under steady state propagation in a model rubber undergoing Mullins softening. The strain energy release rate G is defined as the sum of an intrinsic material parameter G_0, and a dissipative part G_D depending on the amount of energy consumed by Mullins softening upon loading and crack propagation. Such a decomposition is inspired by the same decomposition adopted in order to account for the viscoelasticity of soft materials (see the topical review from Persson et al., 2005). Their theory is developed for an incompressible Neo-Hookean material modified by the Ogden and Roxburgh (1999) model to account for the Mullins softening. Their computational approach aims to estimate the value of G_0. Capitalizing on this remarkable theoretical work, the present study intends to investigate experimentally the resistance to failure of an actual elastomer undergoing Mullins softening, in order to estimate the dissipative part of the energy release rate G_D and address the possible existence of an intrinsic parameter G_0.

For this purpose, thin plates of carbon black filled SBR were manufactured by the French tyre manufacturer and cut into pure shear test geometries. Fracture tests were run on virgin and preloaded notched samples in order to estimate the contribution of the Mullins energy dissipation on the critical energy release rate. On one side, a simple global energy balance analysis using the experimental macroscopic stress-strain curves provides access to two quantities, the classical global critical strain energy release rate G_c as defined by Rivlin and Thomas (1953), which characterizes the global material resistance to fracture, and the original critical energy release rate G_c^* characterizing the change of stored energy during the crack growth. On the other side, monitoring the local strain using digital image analysis on the free surfaces of the pure shear specimens, allows estimating the data required to calculate G_0 and G_D by following the theoretical analysis of Qi et al. (2018). Moreover, the calculations carried out give access to quantitative separation of the Mullins energy dissipation during the loading driving to the crack propagation, and of the Mullins energy dissipation during crack propagation. This work provides a direct comparison between the theory proposed by Qi et al. (2018) and actual experiments.

2. Experimental characterization of the fracture toughness of a filled rubber with respect to the loading history

2.1. Material and testing

2.1.1. Material

Rectangular plates of styrene butadiene rubber (SBR) filled with 50 phr of N347 carbon-black were manufactured by Michelin. The star-branched solution SBR presents a molar mass of M_n = 120 kg/mol with a styrene content of 15%. Some plates were cut into pure shear geometry samples of 147 mm width, 20 mm height and 2.4 mm thickness without any preloading. Other plates were first submitted to uniaxial tensile tests in order to soften the material by Mullins effect, before cutting the same pure shear geometry samples. The pre-stretch softening loadings were applied once only.

2.1.2. Applied pre-stretching

The amount of uniaxial stretching undergone by the plates was monitored by dots tracking on the free surface of the plate (Figure 1). The in-plane components of the deformation gradient tensor $\mathbf{F}$ are calculated on each dot position using a method inspired by the finite element discretization. First, a mesh is created using a Delaunay triangulation with the dots as apexes thanks to SciPy python tools (Jones et al., 2001). For each element, homogeneous values of the deformation gradient are calculated according to the displacements of its nodes using first order Lagrangian shape functions. The deformation gradient at each material point is then computed as the average of the deformation gradient values of each element having the material point as a node, and weighted by its surface. Thanks to this procedure, the deformation gradient fields resulting from the tensile test are displayed in Figure 2a, showing a good

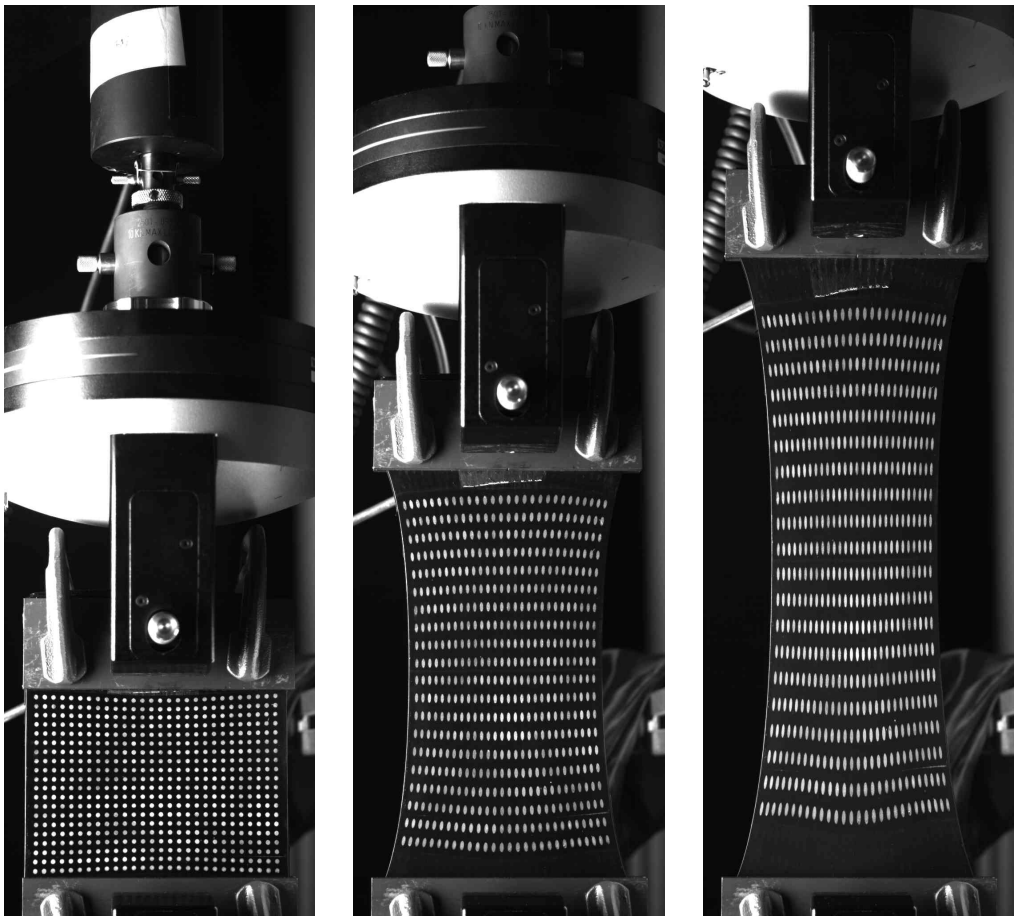

(a) (b) (c)

Figure 1. Material plate of width 147 mm (a) unloaded and submitted to (b) 100% uniaxial local stretch (c) 200% uniaxial local stretch.

homogeneity in a large area of the plate, allowing the cut of two pure shear samples for each plate (Figure 2b) for which similar pre-stretchings are reasonably assumed. Moreover, a similar particle tracking method has been shown to be well suited for the problem of crack opening at large deformation (Qi et al., 2019).

2.1.3. Pure shear fracture tests

The pure shear tests are simply completed on the pure shear geometry by applying a uniaxial tensile loading along the height direction. Tests are run on an Instron 5882 tensile machine equipped of a 2 kN load cell and the crosshead speed is maintained constant at a low value of 5 mm/min in order to limit the possible viscoelasticity. Figure 3 shows the stress-stretch responses of the virgin material and the same material earlier submitted to 100% or 200% uniaxial stretching in the same direction as the current loading (Figure 1). The different stress-stretch responses illustrate the material Mullins softening depending on the loading history. Note that the actual contribution focuses on the Mullins softening occurring when the material is submitted to a level of strain never undergone yet. Further fatigue softening may happen in the case of cyclic loading (Merckel et al., 2011) and could be considered similarly.

For fracture toughness characterization, a notch of either 40 mm or 50 mm was made manually with a razor blade in the middle of the left edge of each pure shear geometry as illustrated in Figure 2b. The free surface of the sample was marked with a regular grid of white dots of 0.75 mm diameter reaching a density of 0.6 dot/mm^2. Images of the pure shear fracture tests were recorded with a camera of 2048 $\times$ 2048 pixels resolution and an acquisition frequency reaching up to 75 images per second. The state of deformation measured on the free surface of a notched sample by dots tracking, is displayed in Figure 4 in terms of the invariants h_{eq} and ρ of the Hencky (1931) tensor,

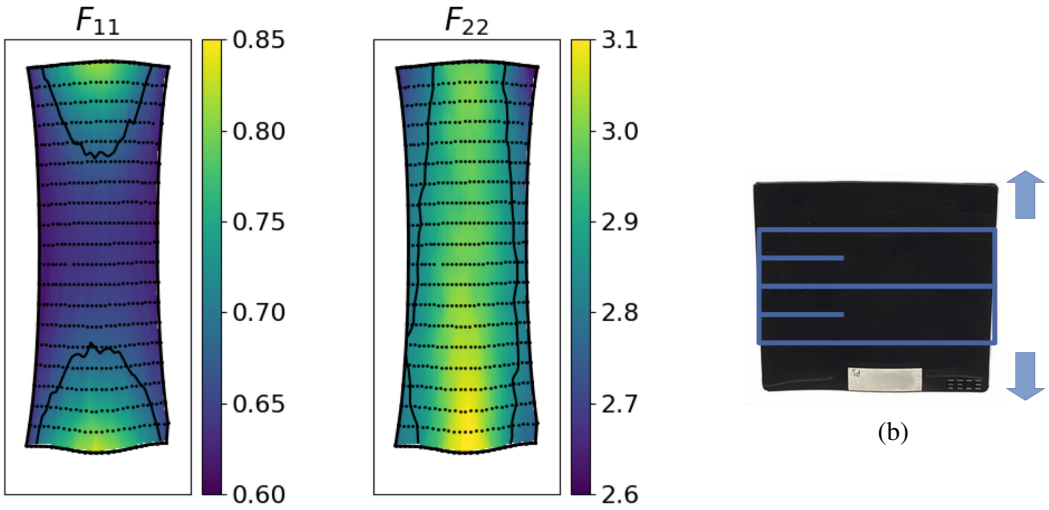

(a)

Figure 2. (a) Deformation gradient fields in directions transverse to the stretching F_{11} and along the stretching F_{22} resulting from analysis of images recorded during test Figure 1. The solid lines delimit values varying from more than 5% from the value at the center of the sample. (b) Illustration of the location for the cut of the pure shear samples after pre-strectching.

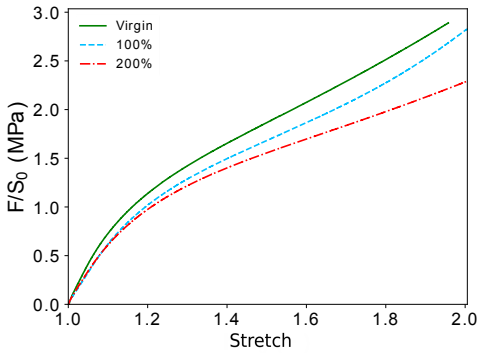

Figure 3. Illustration of the Mullins softening: Pure shear stress-stretch responses for the virgin material and for the material previously submitted to 100% or 200% stretching in the same direction as the current loading.

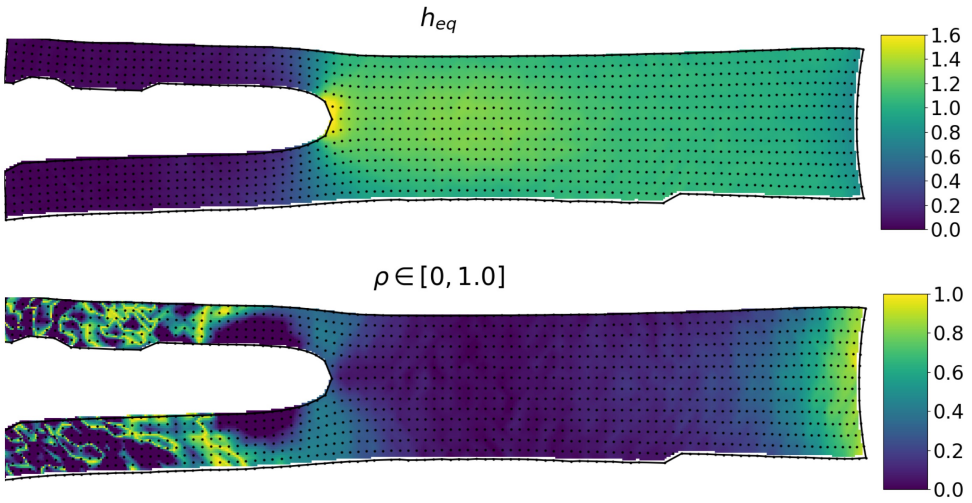

Figure 4. Invariants of the Hencky tensor characterizing the intensity (h_{eq}) and the state (ρ) of loading measured during a fracture test validating the sample pure shear state during crack propagation.

$\mathbf{h} = (1/2) \ln \mathbf{F}.\mathbf{F}^T$. Noting $h_1 \geq h_2 \geq h_3$ the principal invariants of $\mathbf{h}$, $h_{eq} = \sqrt{2/3\,(h_1^2 + h_2^2 + h_3^2)}$ and $\rho = 3h_2/(h_3 - h_1)$ characterize the intensity and the state of loading respectively. One notes that ρ is null in the region in front of the crack tip, corresponding to a desired pure shear state of deformation.

2.2. *Impact of the loading history on the material fracture*

For each loading history, virgin material, pre-stretched at 100% and pre-stretched at 200%, ten notched pure shear samples were tested until break. Figure 5 shows the stress-stretch response until break of every tested sample. First, the stress increases as the notch opens elastically without creating new crack surfaces. Second, the stress declines increasingly as the crack progresses slowly, creating new rough surfaces. Finally, the crack propagates catastrophically, illustrated by a nearly vertical drop in the stress-stretch response.

Following the classic analysis of Rivlin and Thomas (1953), the strain energy release rate for pure shear geometries is calculated from Figure 5 according to,

$$G(\lambda) = W_{PS}(\lambda) h_0 \tag{1}$$

with h_0 the initial height of the sample, $\lambda = h/h_0$ the current stretch, and W_{PS} the material elastic stored energy density when submitted to pure shear. The critical strain energy release rate G_c is defined as the value of $G(\lambda_c)$ with λ_c the stretch at catastrophic break. While λ_c is extracted from figure 5, $W_{PS}(\lambda_c)$ is obtained from Figure 3. The resulting stretch at break and critical energy release rate are displayed in Figure 6 in terms of Tukey (1977) box plots (see Appendix A for a reminder of such a representation). The values of λ_c and G_c must be considered together since they are not independent, the second one being determined from the first one. The values of λ_c are remarkably similar, and one may notice that the initial crack length does not affect λ_c. Consequently, the values of G_c depend significantly on the sample loading history due merely to the softening recorded in Figure 3. The experimental values of λ_c and G_c that have been used to draw Figure 6 are listed in Appendix B for the reader interested in doing his own statistics. Note that the onset of the crack propagation could have been chosen instead of the stretch at catastrophic failure. This would have drawn more uncertainty on the values of λ_c that are easier to pinpoint when dealing with the catastrophic failure due to the significant instantaneous drop of the stress (Figure 5). Moreover, it seems that the stretch at fracture onset, when recognized as the stretch at which the stress-stretch response initiates its downward fall, follows the same trends as λ_c, being independent of the preloading.

In order to show that G_c is a material parameter that does not depend on the geometry of the pure shear sample to the contrary of λ_c, the same pure shear fracture tests were run on two supplementary geometries for the virgin material. The second geometry, noted VG_s2, has the same dimensions as the initial geometry (VG_s1) except for

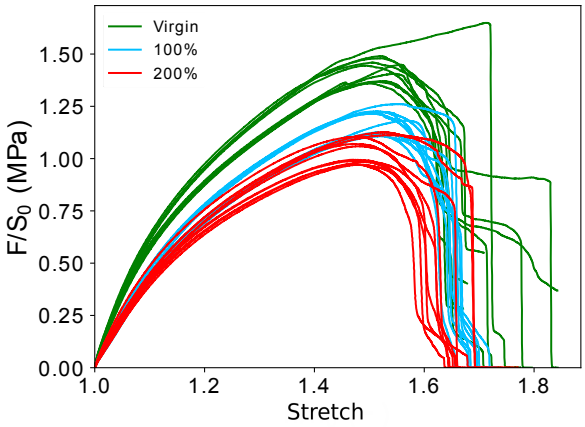

Figure 5. Pure shear notched samples stress-stretch until break according to the stretching history.

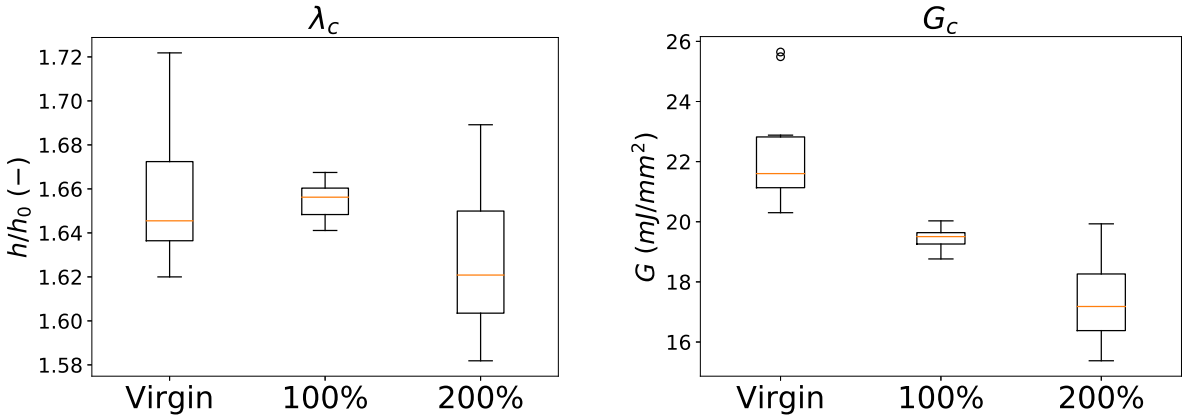

(a) (b)

Figure 6. (a) Stretch at break and (b) critical strain energy release rate according to the loading history, virgin material and material softened by previous stretches at 100% and 200% in the direction of the loading. See Appendix A if not familiar with the Tukey representation.

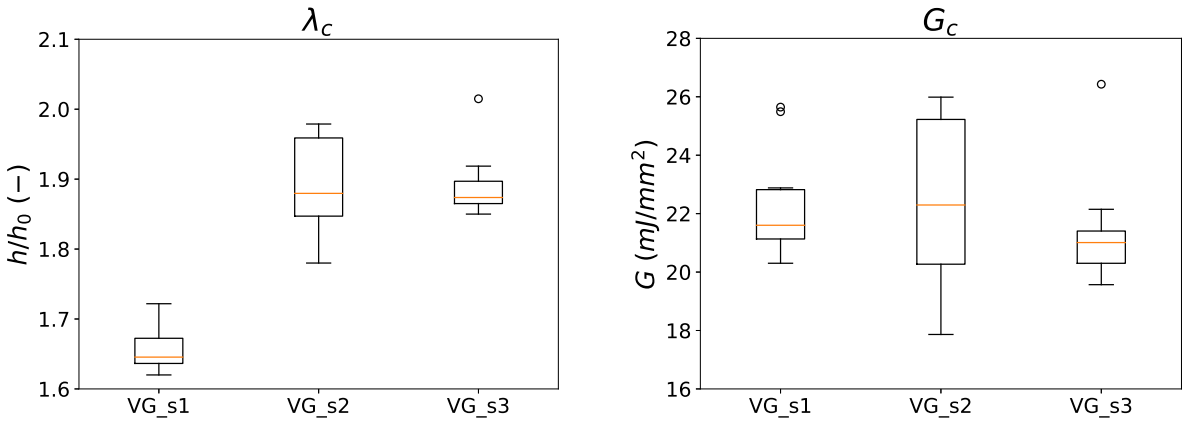

Figure 7. (a) Stretch at break and (b) critical strain energy release rate according to the geometry of the pure shear sample

its height that has been divided by two, and the third geometry (VG_s3) has both height and width divided by two compared to the initial geometry. Figure 7 shows the stretch at break and critical energy release rate for the three pure shear geometries. One notes that the stretch at break depends on the initial height of the specimen but not on its width, while values of G_c recover with a similar median value. With similar values of G_c, Equation (1) explains why λ_c depends on the material behavior and h_0.

Therefore, it was observed that the critical energy release rate does not depend on the geometry of the pure shear sample but changes significantly with the loading history of the material. This raises the question of how to predict the crack propagation in such a material. A notched sample of virgin material consumes parts of the energy for the Mullins softening, and therefore violates the elasticity assumption used by Rivlin and Thomas (1953). The next section takes into account the energy dissipation by the Mullins softening in the definition of the critical energy release rate for the creation of new surfaces.

3. Material fracture toughness vs. energy dissipation during crack propagation

3.1. Theory

The theory developed by Rivlin and Thomas (1953) driving to Eq. (1) has been established for non-dissipative hyperelastic materials based on the classic fracture energy balance made through the virtual steps:

(I) Loading the specimen up to a global displacement L_c without crack propagation allows characterizing the energy put into the system.

(II) While the global displacement is maintained constant at L_c, the crack propagates of a small length da and stops, the crack new length becomes $a + da$. Part of the mechanical energy has been consumed by the creation of new surfaces of the crack.

(III) Unloading the specimen, the elastic energy remaining in the specimen is restituted allowing the calculation of the energy consumed during the crack propagation.

In the case of actual fragile materials, since a controlled crack growth of da only is not possible, Rivlin and Thomas (1953) proposed ingeniously to compare the energy stored during the loadings of specimens of crack length a and of crack $a + da$ to reach the desired energy balance. The same approach was considered in the previous section for carbon-black filled rubber specimens undergoing energy dissipation due to the Mullins effect and requires a more careful analysis. When specimens are loaded to the given displacement L_c, only part of the external energy is stored, the rest being dissipated by the Mullins effect. Therefore, when considering a specimen with crack length a, one

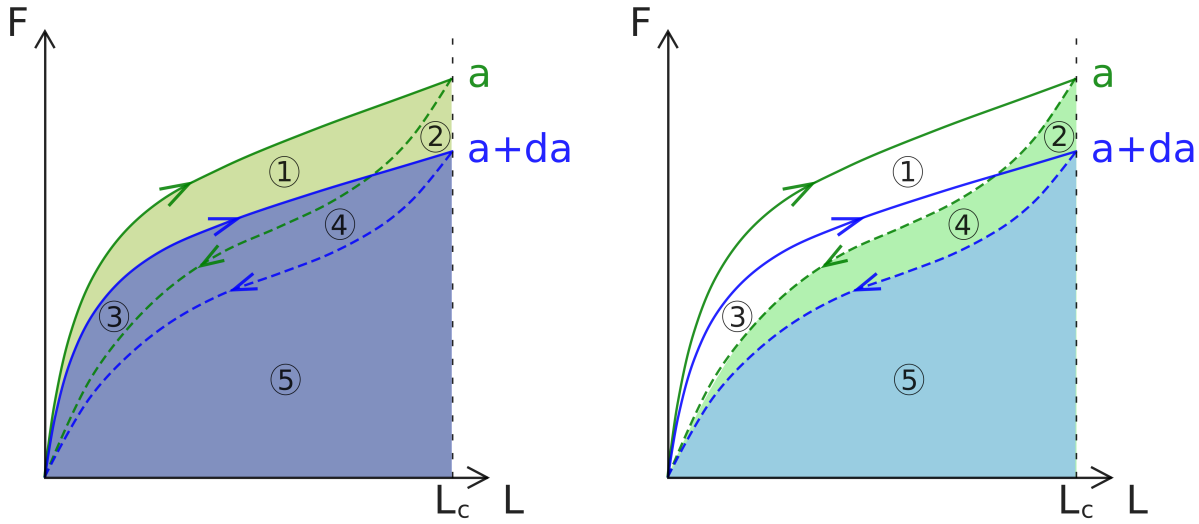

(a) (b)

Figure 8. Illustration of the energy balance, observed during the extension of a crack from a to $a + da$ of an initially virgin specimen undergoing some Mullins softening, which is used to estimate the strain energy release rates G (a) and G^* (b).

has to consider the external work put in the system and the virtual unloading response corresponding to the elastic stored energy. These quantities are presented in Figure 8 for both specimens of crack lengths a and $a + da$, the solid line curves correspond to the external work needed to reach the global displacement L_c, and the dotted line curves designate the stored elastic energy available once L_c is reached.

In order to clearly describe the relevant energies in play during the process of crack length extension, several areas have been labeled from 1 to 5 in Figure 8. In particular, the global external work balance is defined by the area between the two solid lines,

$$U_{ext}(a+da) - U_{ext}(a) = dU_{ext} \quad \text{i.e.} \quad \left(③+④+⑤\right) - \left(①+②+③+④+⑤\right) = -\left(①+②\right) \tag{2}$$

However, since the material dissipates energy through Mullins softening, this energy balance does not characterize the energy consumed by the fracture process only. Upon the loading of specimen of crack length a, the energy loss by Mullins softening appears as the sum of area ① + ③ in Figure 8, and therefore the stored elastic energy $U_{elas}(a)$ is delimited by area ② + ④ + ⑤. Assuming that the crack propagates to reach $a + da$, the area under the unloading dashed line curve for configuration $a + da$, i.e. area ⑤ designates the elastic stored energy $U_{elas}(a + da)$ in the specimen at global displacement L_c, after the crack has propagated. Therefore the energy used by the crack to expand from a to $a + da$ is given by:

$$U_{elas}(a+da) - U_{elas}(a) = dU_{elas} \quad \text{i.e.} \quad \left(⑤\right) - \left(②+④+⑤\right) = -\left(②+④\right) \tag{3}$$

As a consequence of this energy balance analysis, two strain energy release rate quantities can be derived from Eqs. 2 and 3, by considering the external work or the elastic stored energy:

$$G = -\frac{1}{t}\frac{\partial U_{ext}}{\partial a}\Big|_{L=L_c} \tag{4}$$

and

$$G^* = -\frac{1}{t}\frac{\partial U_{elas}}{\partial a}\Big|_{L=L_c} \tag{5}$$

These two quantities, as discussed in Qi et al. (2018) through a thermodynamically based approach, are rather complimentary. Material parameter G characterizes the variation of external energy that has to be provided to witness the growth of the crack and can be considered as the global material resistance to an external solicitation. Meanwhile, material parameter G^* determines the decrease of elastic stored energy per unit area of created surface during the crack growth. The two quantities differ by including or excluding the Mullins softening energy dissipation, which can be seen as an additional contribution to crack growth resistance. Note that the notations G and G^* adopted in the current contribution are different from Qi et al. (2018), G being easily accessible experimentally following Rivlin and Thomas (1953) approach, while G^* requires to know the softened behavior of the material.

The previous considerations were made for a virgin sample, for which the Mullins effect is activated during the first load. However, the reasoning still applies for preloaded specimens, with the loading curves being modified accordingly. In particular, in the case of a sufficiently large preload, the Mullins effect may not be activated leading to the simple case where $G = G^*$. In the next section, the values of G^* are estimated and compared to the values of G for the tests run in section 2.2.

3.2. Theoretical estimate of G^*

In order to calculate G^*, one needs to define the strain energy density that reproduces the mechanical behavior of the material with an account for the Mullins softening. Such a behavior measured in pure shear was displayed in Figure 3. To simplify the purpose, a mere isotropic Neo-Hookean strain energy density is chosen,

$$\mathcal{W}^{NH}(\mathbf{F}) = \frac{\mu}{2}(I_1 - 3), \tag{6}$$

I_1 being the first invariant of the right Cauchy-Green tensor $\mathbf{C} = \mathbf{F^T F}$. In order to account for the Mullins softening, a damage parameter D is classically introduced, and the damaged material stored energy becomes,

$$\mathcal{W}(\mathbf{F}, D) = (1 - D)\mathcal{W}^{NH}(\mathbf{F}). \tag{7}$$

Knowing that the Mullins softening depends on the maximum applied loading (Mullins, 1969), D is defined as a function of I_1^{max}, the maximum value of I_1 recorded over time. In order to reproduce well the stress-stretch response shown in Figure 3, the following expression is proposed for D,

$$D(I_1^{max}) = \frac{\alpha(I_1^{max} - 3)^\beta}{1 + \alpha(I_1^{max} - 3)^\beta}, \tag{8}$$

with $D = 0$ in the initial state when $I_1^{max} = 3$, and D increasing toward its limit value of one when the maximum applied load increases. Figure 9a shows a satisfactory comparison between the experimental data and the simple model responses for parameter values: $\mu = 2.17$ MPa, $\alpha = 0.40$ and $\beta = 0.32$.

Using the critical stretch at break λ_c measured experimentally, and following the same logic as Rivlin and Thomas (1953) to calculate G according to Eq. (1), the critical strain energy release rates G_c and G_c^* are calculated just as,

$$G_c = \mathcal{W}(\lambda_c, D_{preload})\, h_0 \qquad D_{preload} = max_{preload}(D) \tag{9}$$

$$G_c^* = \mathcal{W}(\lambda_c, D_{max})\, h_0 \qquad D_{max} = max_{\tau}(D) \tag{10}$$

where $max_{preload}$ characterizes the maximum value over the preloading history (before a notch is made) and max_τ indicates the maximum value over the whole loading history including the loading applied on the notched sample.

Figure 9b compares the theoretical values of G_c and G_c^* and the values of G_c previously calculated with the experimental data (Figure 6) for the different stretching histories. First, one notes that the theoretical values of G_c reproduce well the experimental estimates for the virgin material and the material pre-stretched at 100%. For the case of 200% of pre-stretching, the theoretical values underestimate the experimental values due to fact that the model stress-stretch response appears below the actual material response for stretches below 1.5. Despite this discrepancy, the model reproduces well the general trend displayed by the experimental data in terms of the changes of G_c with respect to the stretching history. Second, for the virgin material, the Mullins softening evolves from the beginning of the loading, applying as a source of energy dissipation, and resulting in smaller values of G_c^* than G_c. For the pre-stretched specimens, the stretches of 100% and 200% are larger than the critical stretch values λ_c. Consequently, the

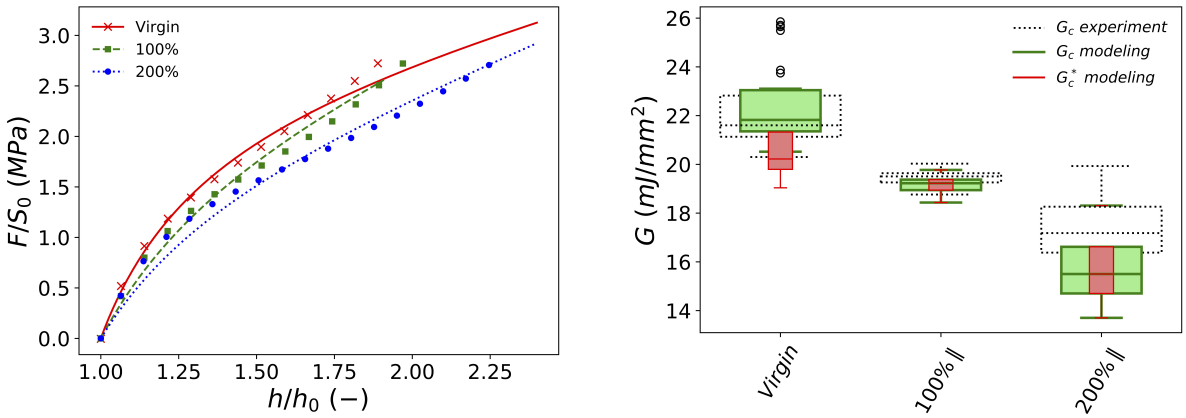

(a) (b)

Figure 9. (a) Fit of the Mullins softened pure shear stress-stretch responses (symbols) with the model (solid lines) defined by Eqs (6-8). (b) Comparison of the theoretical strain energy release rates G_c and G_c^*, calculated for the model parameters defined by the fit displayed in (a), and the values of G_c calculated with the experimental data for the different loading histories.

Mullins effect is not activated during the fracture tests and the theoretical estimates of G_c and G_c^* coincide. One notes in Figure 9b that, similarly to G_c, the material parameter G_c^* is affected by the loading history, meaning that the energy used by the crack when it grows, depends on the material loading history. This raises the question of the occurrence of more energy dissipation by Mullins softening upon crack propagation. The next section explores this question by applying the Qi et al. (2018) theoretical framework to our experimental results enriched of the local displacement recorded during the pure shear fracture tests.

4. Intrinsic toughness and dissipation by Mullins effect

4.1. Theory

The framework introduced by Qi et al. (2018) considers the existence of an intrinsic material parameter G_0, which characterizes the rate of energy consumed exclusively by the creation of new crack surfaces. By definition, such a parameter is independent of any other bulk energy dissipation process such as the Mullins effect, and the total material toughness G_c decomposes as $G_c = G_0 + G_d$, where G_d represents the additional contributions to fracture resistance caused by other dissipation processes.

Keeping in mind the loading steps (I) to (III) and the critical strain energy release rates G_c and G_c^* discussed in section 3.1, the quantity $G_d^I = G_c - G_c^*$ is now introduced. By definition, G_d^I is associated with the energy dissipated by Mullins effect during the loading step before the crack propagation, *i.e.* during step (I). The additional dissipation caused by Mullins effect happening during the crack propagation step (II), is now noted G_d^{II}, leading to the following decomposition:

$$G_c^* = G_0 + G_d^{II} \tag{11}$$

Such a decomposition could explain the dependence of G_c^* on the preloading history that has been experimentally observed in section 3.2. The parameter G_0 is of considerable interest since it may constitute a prime candidate as a crack propagation criterion for materials presenting Mullins effect, granted that it does not depend on the loading history.

The quantity $G_d = G_d^I + G_d^{II}$ encompasses both energy dissipations occurring during the load and the crack propagation, and may be considered as the total supplementary dissipation term. It also enables to write:

$$G_c = G_0 + G_d \tag{12}$$

which is in line with (Qi et al., 2018) postulate.

Considering the pure shear specimen tests carried out on the carbon-black filled SBR presenting substantial Mullins effect, and very limited rate-dependance at the low strain rate applied, the quantity G_d is estimated using the local displacement measured experimentally and reproducing the theoretical calculations from Qi et al. (2018). The directions of crack propagation and of the specimen height are noted X and Y respectively, the dissipation term G_d can be computed through a volume integration:

$$G_d = \int_{Y=-h_0/2}^{+h_0/2} \int_{X=-\infty}^{+\infty} \phi(X,Y)\, dXdY \tag{13}$$

with ϕ the energy dissipated by the Mullins softening, per unit volume and per unit advance of the crack. The crack is assumed to propagate in a steady state. Therefore, considering a forward motion of length da of the crack is equivalent to consider a backward motion of da of material point M as illustrated in Figure 10. Moreover, the specimen is assumed long enough to avoid considering the edge effects. As shown by Qi et al. (2018), the integration (Eq. 13) may be simplified by the summation over the variable X for the material points at the same given height Y_0. Along axis $Y = Y_0$, it is assumed that the strain increases as the point gets closer to the crack tip, until reaching a maximum value at position X_{max} depending on Y_0. An illustration of the value of $\mathcal{W}(X, Y_0)$ is given in Figure 10. Far from the crack tip, the material response is defined by the pure shear state and is noted $\mathcal{W}_{PS}$. Due to the account of the Mullins softening, this quantity depends on the material history of loading. Considering, the model proposed in Eq. (7), for which the Mullins softening is activated upon loading, G_d is now simply evaluated with,

$$G_d = \int_{Y=-h_0/2}^{+h_0/2} \int_{\mathcal{W}_{max}}^{\mathcal{W}_{PS}} \tilde{\phi}(\mathcal{W}, Y)\, d\mathcal{W}dY = 2 \int_{Y=0}^{+h_0/2} \Big(\mathcal{W}(\mathbf{F}(Y), D_{max}(Y)) - \mathcal{W}(\mathbf{F}(Y), D_{preload}(Y)) \Big) dY, \tag{14}$$

where for any height Y, the quantity $D_{max}(Y)$ is the maximum value of the damage witnessed along axis X over time, covering the preloading and fracture test, and $D_{preload}(Y)$ is the maximum damage reached during the preloading history only. This expression is similar to Eq. (26) in Qi et al. (2018) but extended to the material constitutive equations considered in the present study. Note that Eq. (14) is valid whether the material is initially virgin ($D_{preload} = 0$) or already softened ($D_{preload} \neq 0$), and requires the knowledge of the local strain fields. The next section aims to calculate G_d with respect to the preloading history based on the local strain fields evaluated on the free surface of the pure shear specimens during the fracture tests.

4.2. Experimental estimate of G_d

Before comparing the results for every testing condition, the experimental procedure is first detailed on a representative sample of virgin material. When the crack propagation speed is too high, which is the case when $G = G_c$, the local displacement fields could not be computed at the crack tip, due to failure of the dot tracking algorithm. Therefore, the local deformation gradient fields have been computed at a slightly lower global stretch of $\lambda = 1.59$ instead of $\lambda_c = 1.64$, which explains why the values of G_c presented in this section are lower than the previous ones. However, this small underestimation does not affect the reasoning behind the results.

The computed deformation gradient field $\mathbf{F}$ allows calculating the strain energy field $\mathcal{W}(\mathbf{F}, D)$ that is shown in Figure (11). For each height Y, the maximum value of $\mathcal{W}$ over the width X, $\mathcal{W}_{max}(Y) = \max_{\{X\}} \mathcal{W}(X, Y)$, is highlighted in red. The red dots display a symmetric u-shaped curve within the accuracy of measurement, which is in accordance with the parabola predicted theoretically and numerically by Qi et al. (2018).

The profile of $\mathcal{W}_{max}(Y)$ is displayed in Figure 12a. It shows a satisfactory symmetry around the axis defined by $Y = 0$ that corresponds to the crack tip. Far from the crack tip at $Y > 5$ mm, a plateau value noted $\mathcal{W}_{PS}$ is observed for $\mathcal{W}_{max}(Y)$. As predicted by Qi et al. (2018), the value $\mathcal{W}_{PS}.h_0 = 18.7$ mJ/mm^2 is remarkably close to the global value of $G_c = 19.0$ mJ/mm^2 obtained with Rivlin and Thomas (1953) estimate. Near the crack tip (when $|Y| \to 0$), due to the limited resolution of the mesh, some information is unavailable. Actually, only the displacement field inside the black contour shown in Figure 11 is obtained reliably, and the crack tip is outside this region. Therefore, artifacts are obtained near $Y = 0$ when the actual maximum of $\mathcal{W}(Y)$ is outside the measured boundaries. A simple extrapolation, defining an upper bound of the actual values of $\mathcal{W}_{max}(Y)$ near the crack tip, is proposed in Figure 12b. In their theoretical work, Qi et al. (2018) predicted decrease of $\mathcal{W}_{max}(Y)$ proportional to $1/Y$, which does not apply to the

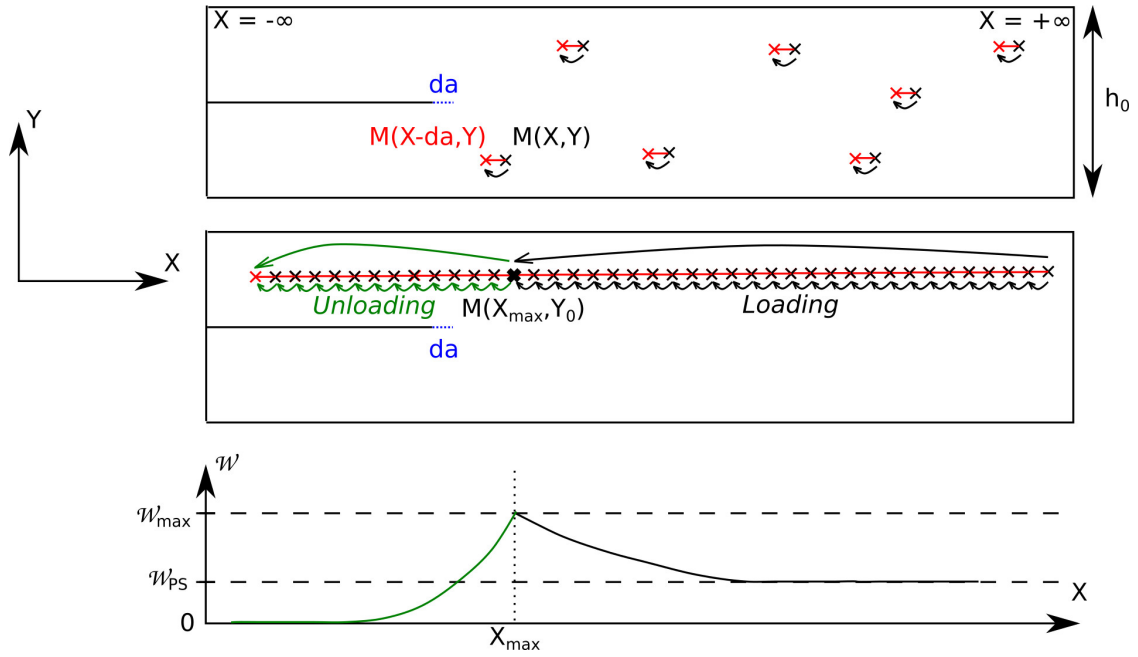

Figure 10. Illustration of (top) the equivalence of the forward displacement of the tip of the crack, (middle) for a given height Y_0, simplification of the material displacement, (bottom) Strain energy density value for a material point M at height Y_0 with respect to X.

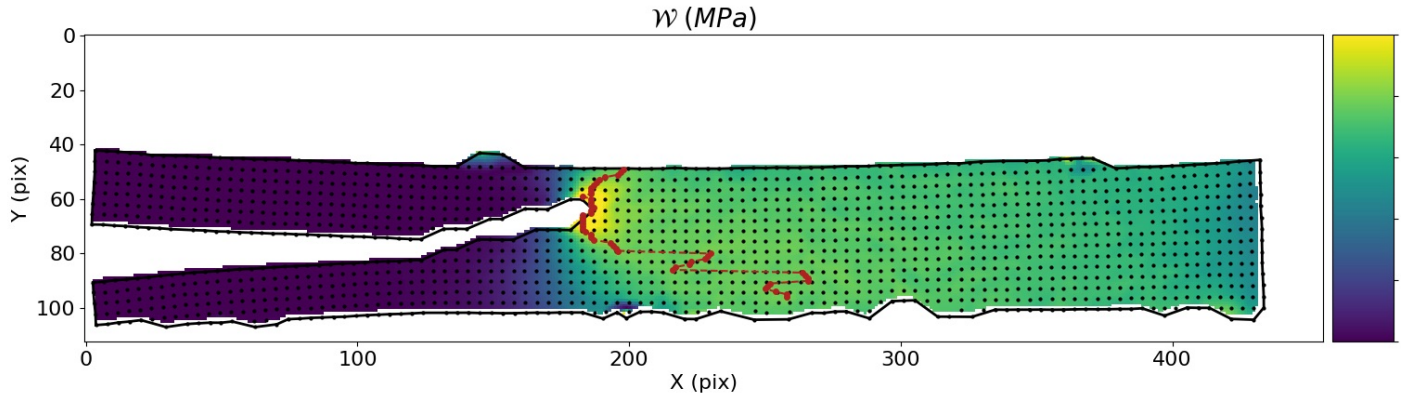

Figure 11. Strain energy density $\mathcal{W}$ field. The red dots define the maximum values $\mathcal{W}_{max}(Y) = \max_{\{X\}} \mathcal{W}(X, Y)$.

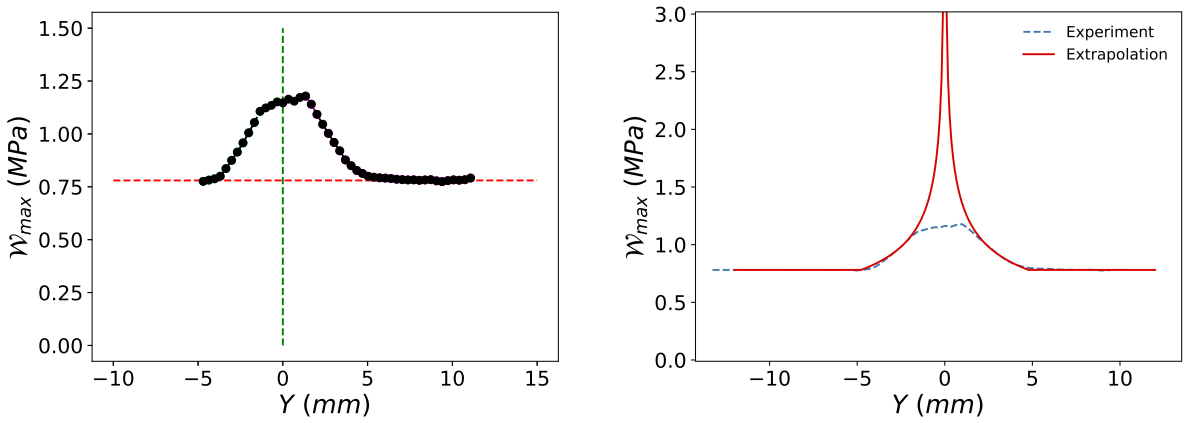

(a) (b)

Figure 12. Values of $\mathcal{W}_{max}(Y)$ with respect to Y (a) extracted from Figure 11 and (b) with a conservative extrapolation near $Y = 0$ where values of I_1 are underestimated.

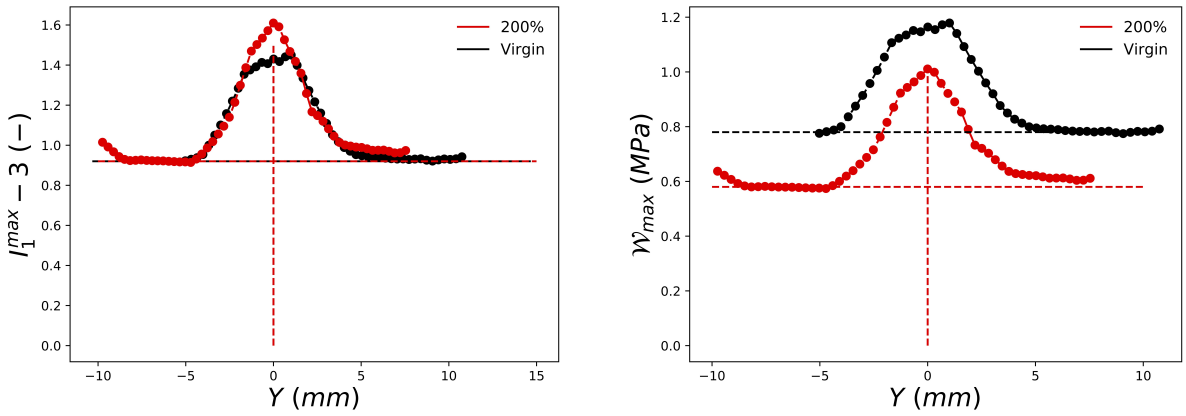

(a) (b)

Figure 13. Maximum values of (a) $I_1 - 3$ and (b) $\mathcal{W}$ over X with respect to height position Y.

experimental measures. However, a power law of the form $C_1(Y_i/Y)^{C_2}$, with $Y_i = 1$mm for the purpose of dimension, $C_1 = 0.3$ MPa and $C_2 = 0.35$ provides a good representation of the experimental data (Figure 12b). This extrapolation diverges when $Y \to 0$, and a cutting value W_{rup} is adopted. The maximum strain energy value measured on a unotched specimen before break in monotonic uniaxial tension is chosen for W_{rup} and a value of 38 MPa has been obtained for the material of interest. The extrapolated profile is then introduced in Eq. (14) in order to calculate G_d. Additionally, G_c and G_d^I are estimated using the global expressions from section 3.2, and every quantity of interest G_c, G_d^I, G_d^{II}, and G_0 can now be evaluated. Note that the same procedure has been applied to samples pre-softened by the Mullins effect. The result obtained on a representative example dealing with a specimen pre-stretched at 200%, is compared to the case of the virgin material presented in Figure 12. Interestingly, the local strain fields within the measured area are similar, as illustrated by the values of $I_1^{max}(Y) - 3$ with respect to Y displayed in Figure 13a. Consequently, the difference between the maximum values of strain energy $\mathcal{W}_{max}(Y)$ between both cases, displayed in Figure 13b, is only due to the material softening. This local observation echoes with the global results on λ_c and G_c discussed earlier.

For each condition of loading history, virgin material, 100% uniaxial pre-stretch and 200% uniaxial pre-stretch, four samples were analyzed. The mean values of G, G_d^I, G_d^{II} and G_0 are listed in Table 1. Because of the relatively low

Table 1. Mean and extreme values of quantities G calculated with the data recorded during pure shear fracture tests for specimens of virgin material and material softened by pre-stretches at 100% and 200%.

(mJ/mm^2)		Virgin	100%	200%
G_c	Mean	20.1	18.0	14.1
	Min	18.7	17.6	13.9
	Max	21.1	19.2	14.6
G_d^I	Mean	1.5	0.	0.
	Min	1.3	0.	0.
	Max	1.6	0.	0.
G_d^{II}	Mean	0.6	0.9	0.2
	Min	0.3	0.4	0.0
	Max	1.4	1.2	0.5
G_0	Mean	18.1	17.2	14.0
	Min	17.0	16.4	13.7
	Max	19.3	18.9	14.5

number of tests, the averages obtained may not be statistically representative, and the extreme values are also given to provide more insight. For both pre-stretched material cases, the applied pre-stretch was larger than the value reached during the crack test. Therefore the material behaves elastically far from the crack tip, resulting in negligible values of G_d^I. The values of G_d^{II}, characterizing the energy dissipated by Mullins softening during the crack propagation, are always positive. The decrease of G_d^{II} with the loading history suggest that the higher the intensity of the preload, the less the crack can dissipate energy by the Mullins effect during propagation. However, the estimated values are very small compared to G_c, showing that the energy consumed by Mullins softening during the crack propagation is very limited. Finally, the values of G_0, characterizing the rate of energy consumed through the creation of new surfaces of crack, show a dependance to the loading history. Unlike Qi et al. (2018) theory, this result suggests that the loading history impacts the fracture process, contradicting the assumption of the existence of an intrinsic value G_0 for the fracture of carbon-black filled rubberlike materials.

Two aspects of the present study should be further discussed considering the important conclusion obtained on G_0. First, it was observed that the fineness of the grids drawn on the free surfaces of the pure shear testing specimens could not provide access to reliable values of $I^1_{max}(Y)$ and consequently of $\mathcal{W}_{max}(Y)$ at the crack tip. Nonetheless, the chosen extrapolation fits well the experimental data, and a refinement of the displacement field near the crack tip is unlikely to change significantly the values listed in Table 1. Second, the strain energy density $\mathcal{W}$ representativity was verified in pure shear for loading history up to 200% only, and may be inaccurate at larger strains. For instance, the energy dissipated by the Mullins effect at very large strain may be significantly larger, and despite the small zone involved, this could drive to a larger dependence of G_d^{II} with respect to the applied loading. Then, G_0 might end up independent of the loading history. However, one has to keep in mind that to reach such a conclusion, the Mullins softening would have to increase very steeply at large strain, which is unlikely.

5. Conclusion

The Mullins effect occuring in carbon-black filled rubbers has been known and studied for years, nonetheless, it has long been disregarded within the study of fracture of such materials. Recently, a theoretical approach based on thermodynamics has been proposed by Qi et al. (2018), which also provided numerically predicted results. In order to provide an experimental insight on this subject, an extensive study has been carried out to evaluate the impact of the Mullins softening on the resistance to fracture of a carbon-black filled styrene butadiene rubber. Using the classical notched pure shear geometry, it has been shown that the global stretch at break is independent of the history of loading, while the critical strain energy release rate characterizing the material resistance to fracture is significantly impacted by the history of Mullins softening. This result implies that the classic fracture analysis introduced by Griffith (1921) and extended to rubberlike materials by Rivlin and Thomas (1953) should be applied with caution on such materials. In order to better understand the experimental results obtained, the reasoning behind the latter method has been reused

accounting for the Mullins energy dissipation. The critical energy release rate G_c^* that characterizes the rate of energy consumed during the crack propagation by the appearance of new crack surfaces, was introduced. It contrasts with the classic quantity G_c, which characterizes the total energy that must be furnished for the propagation to occur, including potential dissipative processes. Based on a theoretical strain energy density representing the behavior of the rubber with Mullins softening, G_c^* has been calculated and was shown to depend on the loading history as well. This result asses the difficulty of defining a fracture criterion for these materials, especially if the loading history is not homogeneous.

An original set of experimental data giving access to the local strain fields just before fracture allowed the comparison between experimental reality and the theoretical work of Qi et al. (2018), confirming some of their numerical predictions. Additionally, based on the theoretical approach they proposed, the Mullins dissipation upon crack propagation was estimated. The latter contribution has been shown to be negligible compared to G_c even though the considered material contains 50 phr of carbon-black and therefore displays significant Mullins softening. Finally, the calculations carried out allowed discussing the possible existence of an intrinsic value G_0 characterizing the fracture of carbon-black filled rubberlike materials, which would act as a predictive criterion for fracture when all the other dissipative phenomena are known. For the moment such a value has not been reached. Further investigation is encouraged towards applying the method to other materials, to more complex cases such as accounting for induced anisotropy, or refinement of the method by obtaining local strain closer around the crack tip for instance.

Acknowledgements

Authors are grateful to Julien Caillard for helpful discussions.

Appendix A. Tukey boxplot / box-and-whisker-plot

A box plot has been adopted to graphically represent the experimental data λ_c and G_c. Figure A.14 shows an example on how a set of values of the critical strain energy release rate are presented, using the following definition:

- Minimum shows the lowest data point excluding any outliers
- First quartile, $Q1$, indicates that 25% of the values of the dataset are below this value
- Median is the middle value of the set of data
- Third quartile, $Q3$, indicates that 25% of the values of the dataset are above this value
- Maximum shows the highest data point excluding any outliers
- The outlier are marked by 'o' symbols

Such a statistical representation is particularly recommended when the set of data is small to moderate. The height of the box represents the interquartile range (IQR) providing an estimate of the dispersion of the data. The outlier values have been estimated as being further than Q_1 and Q_3 of 1.5 times the IQR. Note that the value of 1.5 was set based on the assumption that the variables of interest follow a normal distribution.

Appendix B. Experimental values

The experimental values extracted from the pure shear tearing tests and used for representation of Figures 6 and 7 are listed for the reader's convenience.

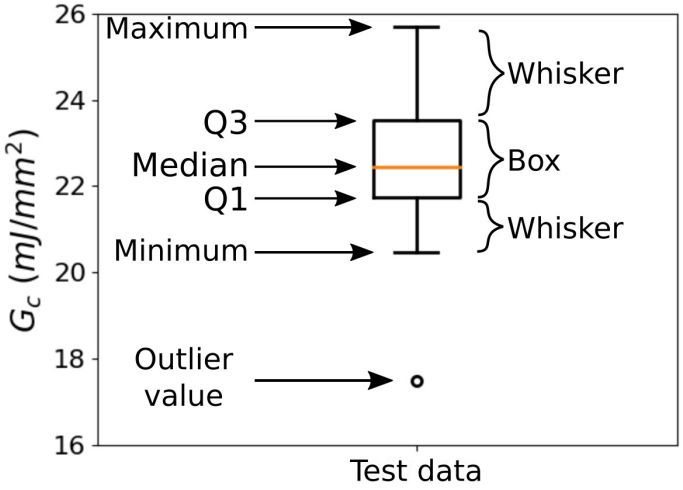

Figure A.14. Illustration of how to read a box plot.

Table B.2. Values of λ_c and G_c (mJ/mm^2) obtained experimentally for each test run according to the experimental conditions.

VG_S1		VG_S2		VG_S3		100%		200%	
λ_c	G_c	λ_c	G_c	λ_c	G_c	λ_c	G_c	λ_c	G_c
1,722	25,65	1,809	18,47	1,853	20,17	1,657	19,43	1,689	19,27
1,715	25,49	1,841	19,89	1,883	21,52	1,652	19,31	1,689	19,93
1,645	21,46	1,866	22,18	1,86	20,13	1,665	20,03	1,63	17,57
1,646	21,74	1,979	25,96	1,85	19,57	1,647	19,24	1,603	16,55
1,642	21,28	1,78	17,86	1,87	20,68	1,667	20	1,622	17,29
1,635	21,08	1,976	25,99	1,874	21,06	1,641	18,76	1,657	18,49
1,62	20,3	1,927	24,08	1,898	21,04	1,661	19,64	1,582	15,38
1,674	22,88	1,969	25,6	1,896	20,98	1,655	19,58	1,595	15,9
1,668	22,64	1,867	21,4	1,873	22,15	1,659	19,63	1,604	16,32
1,623	20,55	1,892	22,41	1,919	26,43	1,646	18,85	1,62	17,07

References

[1] De, D., Gent, A.N., 1996. Tear strength of carbon-black-filled compounds. Rubber Chem Technol. 69, 834-850.
[2] Diaz, R., Diani, J., Gilormini, P., 2014. Physical interpretation of the Mullins softening in a carbon-black filled SBR. Polymer 55, 4942-4947.
[3] Gherib, S., Chazeau, L., Pelletier, J. M., Satha, H., 2010. Influence of the filler type on the rupture behavior of filled elastomers. J. Appl. Polym. Sci. 118, 435-445.
[4] Griffith, A.A., 1921. VI. The phenomena of rupture and flow in solids. Phil. Trans. R. Soc. Lond. A. 221, 163-198.
[5] Hamed G.R., Park, B.H., 1999. The Mechanism of Carbon Black Reinforcement of SBR and NR Vulcanizates. Rubber Chem. Technol. 72, 946-959.
[6] Hencky, H., 1931. The law of elasticity for isotropic and quasi-isotropic substances by finite deformations. J. Rheol. 2, 169-176.
[7] Jones, E., Oliphant, T., Peterson, P., 2001. SciPy: Open Source Scientific Tools for Python. http://www.scipy.org/.
[8] Medalia, A.I., 1987. Effect of carbon black on ultimate properties of rubber vulcanizates. Rubber Chem Technol. 60, 45-61.
[9] Merckel, Y., Diani, J., Brieu, M., Berghezan, D., 2011. Experimental characterization and modelling of the cyclic softening of carbon-black filled rubbers, Mater. Sci. Eng. A 528, 8651-8659.
[10] Mullins, L., 1969. Softening of rubber by deformation. Rubber Chem Technol. 42, 339-362.
[11] Ogden, R.W., Roxburgh, D.G., 1999. A pseudo-elastic model for the Mullins effect in filled rubber. Proc. R. Soc. A Math. Phys. Eng. Sci. 455, 2861-2877.
[12] Persson, B.N.J., Albohr, O., Heinrich, G., Ueba, H., 2005. Crack propagation in rubber-like materials. J. Phys. Condens. Matter, 17, R1071-R1142.

[13] Qi, Y., Caillard, J., Long, R., 2018. Fracture toughness of soft materials with rate-independent hysteresis. J. Mech. Phys. Solids, 118, 341-364.
[14] Qi, Y., Zou, Z., Xiao, J., Long, R., 2019. Mapping the nonlinear crack tip deformation field in soft elastomer with a particle tracking method. J. Mech. Phys. Solids, 125, 326-346.
[15] Rivlin, R.S., Thomas, A.G., 1953. Rupture of rubber. I. Characteristic energy for tearing. J. Polymer Sci. 10, 291-318.
[16] Roucou, D., Diani, J., Brieu, M., Mbiakop-Ngassa, A., 2019. Critical strain energy release rate of rubbers: Single edge notch tension vs. Pure shear tests. Int. J. Frac. 216, 31–39.
[17] Tukey, J.W., 1977. Exploratory Data Analysis. Addison-Wesley Publishing Company.